Q1 **Yasin Khan**
Department of Mechanical and Production Engineering,
Islamic University of Technology,
Board Bazar,
Gazipur 1704, Bangladesh
e-mail: yasinkhan@iut-dhaka.edu

Q2 **Md Tanbir Sarowar**
Department of Mechanical and Production Engineering,
Islamic University of Technology,
Board Bazar,
Gazipur 1704, Bangladesh
e-mail: tanbirsarowar@iut-dhaka.edu

Mahir Mobarrat
Department of Mechanical and Production Engineering,
Islamic University of Technology,
Board Bazar,
Gazipur 1704, Bangladesh
e-mail: mahirmobarrat@iut-dhaka.edu

Md. Hamidur Rahman[1]
Department of Mechanical and Production Engineering,
Islamic University of Technology,
Board Bazar,
Gazipur 1704, Bangladesh
e-mail: mhrahman@iut-dhaka.edu

Q3

Performance Comparison of a Microchannel Heat Sink Using Different Nano-Liquid Metal Fluid Coolant: A Numerical Study

This article presents performance comparison between different liquid metal-based nanofluids termed as nano-liquid metal fluids in a microchannel heat sink to achieve ultimate cooling solutions without sacrificing the compact structure and heavy computing speed. The hydraulic and thermal performance of nanofluids having five different liquid metals (Ga, GaIn, EGaIn, GaSn, and EGaInSn) as base fluid and four different nanoparticles (CNT, Al_2O_3, Cu, and diamond) as solute are evaluated comparing with water-based nanofluids. Three-dimensional flow inside miniaturized channels is predicted using single-phase and two-phase numerical simulations. Numerical models are validated against data obtained from experimental studies from the literature. Three different grids are developed, and several element sizes were compared to obtain the grid independence. Upon evaluation, the study can point out that liquid metal-based nanofluids can generate much superior heat transport characteristics with more than 3.41 times higher heat transfer coefficient compared to conventional water-based nanofluids. GaIn–CNT combination exhibits the best thermal solution possible with a heat transfer coefficient increment of 2.68%, 17.19%, 22.16%, and 2.62% over CNT particle-based EGaIn, EGaInSn, Ga, GaSn liquid metal, respectively, for Re = 750. Considering hydraulic performance, performance evaluation criterion (PEC) has been introduced and Ga-based nanofluids are found to be most effective in this perspective. The effect on overall cooling effectiveness has also been carried out with a detailed particle concentration study. This study paves the pathway of using these extraordinary coolants in mini-/microchannel heat sinks. [DOI: 10.1115/1.4054007]

Keywords: two-phase flow simulation, microchannel heat sink, numerical analysis, nano-liquid metal fluid, micro/nanoscale heat transfer, two-phase flow and heat transfer

1 Introduction

In the last few decades, the process of extraction and dissipation of heat from various kinds of mechanical and electronic devices have gotten tremendous attention. With the rapid advancement of technology, these concerning devices have become smaller and compact. Along with that, the heat transfer area has shrunk quite drastically, which made the conventional heat transfer systems to some extent incompatible. In the context of these adverse situations, heat dissipation technology has evolved manifold and gave rise to minichannel and microchannel heat sinks.

The concept was first materialized by Tuckerman and Pease [1] when they developed the idea of achieving an increased heat transfer coefficient by reducing the hydraulic diameter in the channels. The pioneering work resulted in the introduction of microchannel heat sink that possess numerous benefits without compromising the rate of heat transfer [2,3]. Rather it is seen that a microchannel heat sink is capable of extracting more heat (1000 W/cm^2) [1] when compared to the traditional heat sinks (20 W/cm^2).

The factors linked with the convective heat transfer in a microchannel heat sink are as follows: heat sink geometry, channel aspect ratio, substrate material, and coolant flow. Diverse types of microchannel heat sinks are available in the market. These include wavy fin microchannel, pin-fin microchannel, oblique fin microchannel, and double-layered microchannel [4]. Still, the rectangular cross section has been considered as the most efficient design accounting economic and machining factor [5]. The substrate material is also limited by the factors associated with material properties for stable heat transfer.

Among various methods to increment the heat transfer capabilities of microchannel heat sink, finding high performing coolants can be one of the ways. Most of the microchannel heat sink uses water as the working fluid, but there are very few exceptions that include other cooling media associations. Some researchers have considered using Freon-based refrigerants, but their use has been limited due to environmental impact [6]. To overcome certain ecological limitations, the use of eco-friendly working fluids has got more attention. Flow boiling heat transfer was investigated in a microchannel heat sink using R134a, and it was reported that heat sink wall temperature could be maintained below 30 °C when the mass flowrate is above 1000 kg/m^{2}s with 80 W/cm^2 heat flux [7]. It is apparent that the diversified use of refrigerant as the working fluid has been possible only in the flow boiling mechanism [8,9], and apart from this procedure of heat transfer, the majorly used working fluids are air and water. So, the improvement of these two working fluids has become vital in the advancement of heat transfer in microchannel heat sink, which has been possible by introducing the concept of nanofluids.

Nanofluids are made when nanoparticles (typically 1–100 nm in size) that exhibit excellent chemical stability are suspended uniformly in base fluids [10]. The selection of nanoparticle is critical because they have to show chemical stability, which leads to the use of stable metals like Cu, Ag, Au, or metal oxides, namely, Titania (TiO_2), alumina (Al_2O_3), and different forms of carbon (diamond, CNT) [11]. The study of nanofluids was coined in 1993 by Masuda et al. [12], where the use of Al_2O_3, SiO_2, and

[1]Corresponding author.
Manuscript received September 15, 2021; final manuscript received February 17, 2022; published online xx xx, xxxx. Assoc. Editor: Vinod Narayanan.

TiO_2 as nanoparticles with the base fluid brought a significant change in thermal conductivity and fluid viscosity. Nanofluids have been used in almost all kinds of heat exchangers [13].

The introduction of nanofluids in different heat transfer applications has paved the way for the use of these excellent coolants in minichannel and microchannel heat sinks. Integration of nanofluids in microchannel heat sink has developed a lot of potential in the heat transfer industry because of their better performance when compared to the prevailing options. Among all the possible combinations of nanofluids, the use of Al_2O_3 particles has got the maximum attention across all the platforms of heat transfer. Forced convective cooling performance was experimentally investigated using Al_2O_3/water (1–2% in vol) nanofluid in microchannel heat sink [14], and it was reported that there is a very minute increase in the friction factor, which is very insignificant when compared to the vast reduction in thermal resistance. Heat transfer characteristics were investigated numerically by Kumar and Kumar [15] in an electronic chip heat sink, and it was found that at volume fractions of 0.25%, 0.5%, and 0.75% of Al_2O_3/water nanofluids, the increase in Nusselt number is 9%, 23%, and 37%, respectively, when compared to water. Computational fluid dynamics modeling on thermal performance of Al_2O_3/water was studied to compare single- and two-phase flow [16]. It was seen that the Al_2O_3/water nanofluid combination provided the least thermal resistance when compared against a nanofluid combination of Al_2O_3 with engine oil, glycerin, and ethylene glycol [17]. Although Al_2O_3/water nanofluid provided excellent performance in most studies, their long-time usage modifies the crystallite size [18]. As a result, heat transfer performance is affected. So other potential nanofluids have been used in microchannel heat sinks for further research purposes. Sivakumar et al. [19] used CuO as a nanoparticle and compared the performance of CuO/water and Al_2O_3/water nanofluids. Convective heat transfer in a cylindrical microchannel heat sink was studied using Cu/water nanofluid, where 0.05, 0.1, and 0.3 wt% concentration of nanoparticle was used to enhance the Nusselt number by 17%, 19%, and 23%, respectively, when compared against pure water [20]. Jang and Choi [21] studied the contribution of the diamond (1 vol%, 2 nm) in water as nanofluid in microchannel heat sink and concluded that at fixed pumping power, there is a 10% enhancement in cooling performance compared to pure water. The weight concentration of 0.01% CNT nanofluids has been used in thermal optimization of microchannel heat sink [22], and the result dictated that the application of nanofluid improved the convective heat transfer by 2% at 20 °C, 12% at 30 °C, and 13% at 40 °C. The use of TiO_2/water nanofluid has brought some influential researches. A numerical study [23] recorded a maximum increase of 19.66% in the convective heat transfer coefficient at low Reynolds number when they compared TiO_2-based nanofluid to the pure water. As seen from aforementioned discussions, there have been extensive studies on particle materials and particle size of nanofluids. But as for the base fluid, the study has been limited to water and ethylene glycol mostly. But, to reach the ultimate cooling solution and solving the bottleneck issues caused due to rapid miniaturizing and advancement of electronic chips, exploration of alternate base fluid for nanofluids has become very much requisite.

In search of alternative coolant fluids with excellent thermophysical properties, the concept of using liquid metal as the base fluid in place of the commonly used base fluid has gotten more attention. Because of having a meager Prandtl number, liquid metals have much higher heat conductivity than water and almost all the traditional fluids. Song et al. [24] have discussed the application of liquid metal across various fields of energy. Smither et al. [25] used liquid metal for heavy heat load and obtained remarkable feedback favoring the use of liquid metal. A wide range of research has certified the promising contribution of liquid metal in heat transfer applications. Initially, they have been used in nuclear reactors for cooling [26]. Their introduction in minichannel heat sinks has brought huge advancement in the context of heat extraction and removal. Liu et al. compared cooling performance of water and liquid metal under similar microchannel heat sink conditions. Because of their consistent chemical properties and better electrical conductivity, these fluids can be pumped without the help of any moving mechanism by magnetohydrodynamic[27]. Later on, a comparison work has been carried out by Muhammad et al. [28] to show how various types of liquid metal behaves under multiple substrate materials and varying Reynolds number. Numerical investigation of laminar flow was conducted using liquid metal by Muhammad et al. [29]. Heat transfer performance was investigated by Liu et al. [30] using GaInSn. Liquid metal with ceramic substrate was used in a minichannel heat sink [31]. These have further forged the background for the replacement of traditional fluids with liquid metal. Although liquid metal has a huge upside over other fluids, it experiences inevitable backlash when used in heat sinks because of corrosion or chemical inadaptability [32,33]. Substrate coating with molybdenum, nickel, or tungsten is a vital way to overcome such difficulty [34].

These studies opened the door for a new research topic, incorporating nano-liquid metal fluid as the cooling medium so that we can take advantage of both liquid metal and nanoparticles. This proposed concept ensures a high thermal performance and offers a feasible solution regarding bottleneck issues in electronic chip cooling. Ma and Liu [35] proposed the concept of the nano-liquid metal fluid for the first time, in which the nanoparticles with superior thermal conductivity are added to the liquid metal. Moreover, since the liquid metal has large surface tension, a much larger volume fraction of nanoparticles can be added to the liquid metal, so the nano-liquid metal fluid with outstanding thermal conductivity can be obtained [36]. Therefore, the nano-liquid metal fluid can be expected to be an idealistic medium for the heat transfer process.

Considering the thermophysical properties of nano-liquid metal fluid, it is expected to get excellent thermal performance from these in microchannel heat sinks. This serves as a state-of-the-art technology regarding the cooling solution for miniature electronic components. The present study has investigated a detailed thermal, hydraulic, and overall performance comparison of different conventionally used liquid metals (Ga, GaIn, GaSn, EGaIn, and EGaInSn) and nanoparticle (Al_2O_3, Cu, CNT, and diamond) combinations. Influence of different operating parameters such as applied heat flux, flowrate, flow Reynolds number, and mass concentration of particles on the heat transfer coefficient, friction factor, pressure drop, and overall thermal performance of the system is numerically investigated. The goal is to obtain the most optimal combination of nano-liquid metal fluid for different perspectives of thermal, hydraulic, and energetic considerations.

For our comparison study, first, the thermal and hydraulic performance of different liquid metal-based nanofluids is compared with that of water using the same nanoparticle for the same particle concentration. Then, the effect of different nanoparticles is also studied for different base liquid metal fluids for the same particle concentration. This study provides the nanofluid combination having the highest heat transfer coefficient. Finally, the effect of particle concentration on thermal and hydraulic performance has been studied. This systematic study further paves the way for plausible application of nano-liquid metal fluid in practical experiments.

From our comparison study, we have noticed that GaIn-based nanofluids have displayed the best thermal performance. However, considering the energetic cost of pumping, Ga-based nanofluids displayed the optimal overall performance. In brief, liquid metal-based nanofluids have considerably higher performance than water-based nanofluids irrespective of the Reynolds number. By comparing the effect of different nanoparticles, CNT displayed better performance than other conventional particles. The effect of different volume fractions reveals that, the increase in volume fractions of nanoparticles results in thermal performance increment. However, this increment seems to decrease with increasing volume fractions. The overall performance considering pumping power also shows the same trait. However, with increasing Reynolds number, the benefit of thermal performance increment decreases.

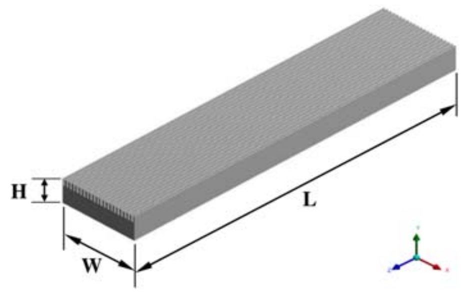

Fig. 1 3D isometric view of the microchannel heat sink

2 Methodology

2.1 Geometric Model. The numerical analysis presented in this study is conducted upon a rectangular microchannel heat sink containing 21 identical channels as shown in Fig. 1. The geometric parameters of the heat sink, presented in Table 1, used in this study are taken from those presented by experimental works done by Ref. [37]. Due to the similar geometry of the channels, the computational domain is taken with three channels as presented in Fig. 2. The top surface of the heat sink was assumed to be having an adiabatic wall, which generates a closed domain for fluid motion inside the mini channels. The study contains a numerical simulation of the fluid flow and heat transfer for a series of Reynolds number. It should be mentioned that the flow Reynolds number never exceeded 1000. Due to which laminar flow regimes could be assumed for all the cases.

2.2 Flow and Thermal Model. This study aims to utilize the most widely used models in predicting thermal and hydraulic performance. From the aforementioned heat sink geometric and input parameters, flow and thermal comparative factors can be calculated.

The friction factor for a single channel can be determined from:

$$f = \frac{\Delta P_c D_h}{2L\rho_{nf} U_{in}^2} \tag{1}$$

where

$$\Delta P_c = P_{in} - P_{out} \quad \text{and} \quad D_h = \frac{4W_c H_c}{2(W_c + H_c)} \tag{2}$$

Now, the overall pumping power required for the forced flow can be calculated from:

$$W = N\Delta P_c A_{in} U_{in} \tag{3}$$

For calculating the heat transfer coefficient, the base fluid temperature difference is considered.

$$\bar{h} = \frac{Q}{N\Delta T_{btd} A_{fin}} \tag{4}$$

where "Q" represents total heat flux at the bottom of the heat sink.

Fin surface area, $A_{fin} = (W_c + 2\eta_{fin} H_c)L_c$ and base fluid temperature difference, $\Delta T_{btd} = \overline{T_w} - 0.5(T_{in} + T_{out})$

$$\eta_{fin} = \frac{\tanh(mH_c)}{mH_c} \tag{5}$$

$$m = \sqrt{\frac{2h}{k_s W_{fin}}} \tag{6}$$

So, the Nusselt number can be calculated as follows:

$$\overline{\text{Nu}} = \frac{hD_h}{k} \tag{7}$$

2.3 Thermophysical Properties of the Base Fluid and Nanoparticles. The thermophysical properties of water–Al_2O_3 nanofluid at different volume fractions are presented in Table 2. These properties of the mixtures are essential for using single-phase methodology in predicting the flow and thermal performance.

For the two-phase analysis, properties of the base fluid and particles are required separately. These properties are temperature-dependent functions and considered to be continuous over the entire domain. Base fluid properties are presented in Table 3, and particle's properties are presented in Table 4.

2.4 Mathematical Formulation. The study consists of two different approaches of numerical models to predict the heat transfer and flow phenomenon inside the microchannels accurately. The governing equations associated with these numerical models are described in this section.

2.4.1 Single-Phase Model. In a single-phase model, the nanofluid is treated as a homogeneous fluid with continuous properties. The differential equations expressing conservation of mass, momentum, and energy are given [38]:

Continuity equation:

$$\nabla \cdot (\rho_{nf} \cdot V_m) = 0 \tag{8}$$

Momentum equation:

$$\nabla \cdot (\rho_{nf} \cdot V_m \cdot V_M) = -\nabla P + \nabla \cdot (\mu_{nf} \cdot \nabla V_m) \tag{9}$$

Energy equation:

$$\nabla(\rho_{nf} \cdot C \cdot V_m \cdot T) = \nabla \cdot (k_{nf} \cdot \nabla T) \tag{10}$$

The selection of suitable correlation to calculate the nanofluid properties plays a significant role in the precision of this model. There is no universal correlation yet, and in studies, they give contradictory results in different circumstances [39]. Nevertheless, all sources indicate that nanofluid properties are dependent on the volume fraction and diameter of particles and dependent on the temperature.

The following formulas are used to calculate nanofluid density, specific heat, viscosity, and thermal conductivity in the present study.

Density [40]:

$$\rho_{nf} = (1 - \varphi)\rho_{bf} + \varphi\rho_s \tag{11}$$

Specific heat [40]:

$$(c_p)_{nf} = \frac{(1 - \varphi)\rho_{bf} c_{p,bf} + \varphi\rho_s c_{p,s}}{\rho_{nf}} \tag{12}$$

Viscosity [41]:

$$\mu_{nf} = \mu_{bf}\left(\frac{1}{(1 + \varphi)^{0.25}}\right) \tag{13}$$

Table 1 Geometric parameter of the MCHS

Material	MCHS height H (mm)	MCHS width W (mm)	MCHS length L (mm)	Channel width W_c (μm)	Base thickness t_b (μm)	Channel wall thickness W_{fin} (μm)	Channel height H_c (μm)
Copper	3.17	10	44.8	215	2349	261.2	821

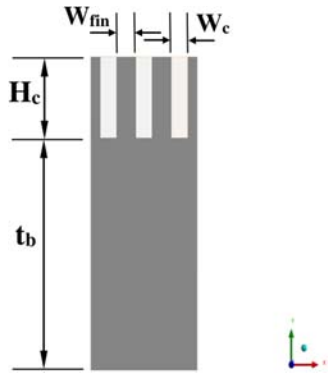

Fig. 2 Front view of the computational domain

Thermal conductivity [41]:

$$k_{nf} = \frac{k_s + (n-1)k_{bf} - (n-1)\varphi(k_{bf} - k_s)}{k_s + (m-1)k_{bf} + \varphi(k_{bf} - k_s)} k_{bf} \tag{14}$$

The particle volume fraction is denoted by φ, and the subscripts s, bf, and nf express particle, base fluid, and nanofluid, respectively. The particles are assumed to be spherical with a shape factor $n=3$.

2.4.2 Two-Phase Model. The two-phase model recognizes the fluid domain as a liquid–solid mixture. There are two computational techniques for modeling such phenomena based on volume fraction. One is the Eulerian–Lagrangian method and another one is the Eulerian–Eulerian model.

The Eulerian–Lagrangian method is used for low volume fraction, whereas the Eulerian method is used to model the base fluid and the Lagrangian method to model the particle flow. Even for a very low volume fraction, the number of particles is very high, making the computational domain's flow prediction pretty impossible by the Lagrangian–Eulerian method due to computing power limitation. This is why the Eulerian–Eulerian model is widely used. The most popular Eulerian–Eulerian methods are mixture, Eulerian and VOF. The difference between the two-phase models' results is marginal [16]. Thus, the mixture model has been selected in the present study due to its simplicity and less computational power requirement with high accuracy to predict the flow [16].

2.4.3 Mixture Model. The mixture model has become popular due to its computational simplicity. Its key feature is that only one set velocity constituent is solved for the momentum conservation equation of the mixture. The effect of the secondary phase on the primary phase via drag force and turbulence is considered. The prior assumptions of the mixture model are as follows:

- Pressure is deemed to be shared equally between phases.
- Particle velocity is extracted from algebraic formulation [42].
- Nanoparticles are assumed to be of spherical shape.
- Phase slip considered for determination of secondary dispersed phase concentration.

The following limitations are associated with the mixture model:

- Compressible property of the mixture is not accounted for.
- Ideal gas law can be employed; hence, pressure boundary conditions cannot be implied.
- The interaction between different dispersed phases is assumed minimum.
- To avoid complexity turbulence generation due to the secondary phase and its effect on the primary–secondary phase, interaction is neglected [42].

The partial differential steady-state governing equations expressing the mixture model are presented as follows [43]:

Continuity equation:

$$\nabla \cdot (\rho_{nf} \cdot V_m) = 0 \tag{15}$$

where V_m is the mass averaged velocity.

Momentum equation:

$$\nabla \cdot (\rho_m . V_m . V_m) = -\nabla p + \nabla \cdot (\mu_m . \nabla V_m) + \nabla \cdot \left(\sum_{k-1}^{n} \varphi_k \rho_k V_{dr,k} \right) - \rho_{m,i} \beta_m g (T - T_i) \tag{16}$$

Energy equation:

$$\nabla \sum_{k-1}^{n} (\rho_k \cdot C_{pk} \cdot \varphi_k \cdot V_k \cdot T) = \nabla \cdot (k_m \cdot \nabla T) \tag{17}$$

Volume fraction equation:

$$\nabla \cdot (\varphi_p \rho_p V_m) = -\nabla \cdot (\varphi_p \rho_p V_{dr,p}) \tag{18}$$

where the mixture velocity V_m, density ρ_m, and viscosity μ_m are, respectively, defined as follows:

$$V_m = \frac{\sum_{k=1}^{n} \varphi_k \rho_k V_k}{\rho_m} \tag{19}$$

$$\rho_m = \sum_{k=1}^{n} \varphi_k \rho_k \tag{20}$$

$$\mu_m = \sum_{k=1}^{n} \varphi_k \mu_k \tag{21}$$

The secondary phase is denoted by "k." The corresponding relative velocity relates to the drift velocity $V_{dr,k}$ of the secondary phase.

$$V_{dr,k} = V_{pf} - \sum_{k=1}^{n} \frac{\varphi_k \rho_k}{\rho_m} V_{fk} \tag{22}$$

Similarly, the nanoparticle's relative velocity (represented by "p") relative to the base fluid (represented by "f") is defined as the slip velocity V_{pf}.

$$V_{pf} = V_p - V_f \tag{23}$$

$$V_{pf} = \frac{\rho_p d_p^2}{18 \mu_f f_{drag}} \frac{(\rho_p - \rho_m)}{\rho_p} a \tag{24}$$

Table 2 Thermophysical properties of water–Al_2O_3 nanofluid

	Water base (φ)					
	0%	1%	2%	3%	4%	5%
K_{nf} (W/m k)	0.603	0.620	0.638	0.656	0.675	0.693
ρ_{nf} (kg/m^3)	995.7	1021.7	1047.7	1073.8	1099.8	1125.9
μ_{nf} (kg/m s)	7.977×10^{-4}	8.177×10^{-4}	8.376×10^{-4}	8.576×10^{-4}	8.775×10^{-4}	8.974×10^{-4}
$c_{p,nf}$ (J/kg K)	4183	4149	4115	4081	4046	4018

Table 3 Thermophysical properties of different base fluids considered for the study

Material	Density ρ (kg/m^3)	Thermal conductivity k (W/m K)	Specific heat c_p (J/kg K)	Dynamic viscosity μ ($\times 10^{-3}$) (Pa s)
Water	995.7	0.603	4183	0.7977
Ga	6090	31	429.9–0.275543T	1.8879
EGaInSn	6440	16.5	295	2.4
EGaIn	6280	26.6	404	1.99
GaSn	6300	30	365	2.192
GaIn	6363.2	39	365.4	2.210

Table 4 Thermal and physical properties of nanoparticles [36]

Particle	Density ρ (kg/m^3)	Thermal conductivity k (W/m K)	Specific heat c_p (J/kg K)
Al_2O_3	3600	36	0.765
Cu	8978	387.6	381
Diamond	3510	1000	497.26
CNT	1600	3000	796

$$f_{drag} = f(x) = \begin{cases} 1 + 0.15\mathrm{Re}_p^{0.687}, & \mathrm{Re}_p \le 1000 \\ 0.0183\mathrm{Re}_p, & \mathrm{Re}_p > 1000 \end{cases} \tag{25}$$

where Reynolds number of nanoparticle "$\mathrm{Re_p}$" and acceleration "a" can be found in the following equations:

$$\mathrm{Re}_p = \frac{V_m d_p}{\vartheta} \tag{26}$$

$$a = g - (V_m \cdot \nabla)V_m \tag{27}$$

2.4.4 Numerical Model. This study contains implementation of different numerical models to accurately predict flow and thermal performance of nano-liquid metal fluid inside a microchannel heat sink. This section presents different numerical methods and boundary conditions used in the study along with the validation of the numerical model with experimental data available in the literature.

The numerical analysis presented in this study was done with ANSYS FLUENT 19. The finite volume method was incorporated to discretize the set of 3D coupled nonlinear differential equations. The SIMPLE algorithm was selected for the pressure–velocity coupling. A first-order upwind method had been used for the convective and diffusive terms. The Gauss–Seidel method was applied in a line going through all volumes in the computational domain to solve the algebraic system that resulted from the numerical discretization.

Single-phase analysis was conducted based on considering the nanofluid as a single-phase fluid, thus utilizing the thermophysical properties of the nanofluid mixture obtained from the existing literature and calculated from theoretical correlations. The analysis following two-phase methodology was conducted by utilizing the thermophysical properties of the base fluid and nanoparticles separately according to different volume fractions of the particles.

Boundary conditions. The following boundary conditions were used in the numerical analysis.

For the solid domain:

Constant heat flux per unit area (q_f = 100 W/cm^2) was applied at the bottom wall ($y = 0$). The symmetry boundary condition was applied at the left and right walls ($x = 0$, $x = W_{fin} + W_c$). The adiabatic wall boundary condition was applied at the top wall, the front, and back wall of the sink ($y = H + t_b$, $z = 0$, $z = L$). No-slip boundary conditions at the fluid–solid interface.

For the fluid domain:

At fluid inlet ($z = 0$), uniform velocity (U_{in}) with constant temperature (T_{in} = 303 K) was applied. Pressure outlet was applied at the fluid outlet ($z = L$).

Validation and mesh independence. The numerical method used in this study was validated against experimental data presented in Ref. [37]. The geometric model explained earlier is being used in the validation. Three different sets of grids were generated for the numerical model. All of the generated grids were used for comparing the solution accuracy with the experimental data. Two factors were considered for the grid test. The first parameter was the accuracy of the grid to reach optimum solution closer to the experimental data. The second thing for consideration was the time required for the solver to reach the convergence. Different grids generated are shown in Fig. 3. The first set of grids contained structured hexahedral cells for both solid and fluid domains. The next grid type contained unstructured tetrahedral cells for solid and fluid domains and the other type of grid contained structured hexahedral cells for fluid domain, while the solid domain contained tetrahedral unstructured cells.

The comparison of numerical results with experimental data presented in Ref. [37] with different grids generated is presented in Table 5. The maximum discrepancy found from the comparison is 3.9%. Although all of the generated grids show very good agreement, the structured mesh generated with hexahedral elements showed less time to reach the convergence. Thus, the grid generated with structured hexahedral elements is selected for the numerical analysis. Two different types of inspection were performed to check the convergence of the numerical analysis. The first one was quantitative convergence, which was checked by monitoring all of the residuals. The other method was to check any variable at any certain boundary of the numerical model, which is termed as qualitative convergence.

To compare the accuracy of the numerical model, the results obtained from the single-phase method and mixture model (two-phase method) are compared with the experimental data as presented in Fig. 4. The following boundary conditions were used for the validation: Q = 100–300 W, T_{in} = 30 °C, fluid mass flowrate = 2.1–5.5 g/s, outlet pressure = 1.12 bar, and coolant used is 2% Al_2O_3–water. Upon comparing the results from single-phase and two-phase numerical models, it is found that two-phase model exhibits better accuracy in predicting the thermal performance of nanofluids in microchannel heat sinks. At Q = 100 W, when the mass flowrate of the coolant is 5.5 g/s, the single-phase and two-phase models showed 11.24% and 5.83% deviation, respectively. At 300 W, when the mass flowrate of the coolant is 5.5 g/s, the associated deviation by single-phase and two-phase models reached 6.97% and 5.52%, respectively. In all of the cases, the errors associated with single-phase and two-phase numerical models did not exceed 12% and 6%, respectively. Thus, for exhibiting better accuracy, two-phase numerical model (mixture model) has been selected for the present study.

3 Results and Discussion

This section presents thermal and hydraulic performance of different liquid metal-based nanofluids in a microchannel heat sink. The thermal performance has been compared through average heat transfer coefficient and substrate wall temperature along the length of microchannels. The hydraulic performance of different coolants is compared by monitoring the pressure drop due to pumping the coolants through the microchannels. Finally, performance evaluation criteria has been explained and utilized to compare liquid metal-based nanofluids with water-based nanofluids.

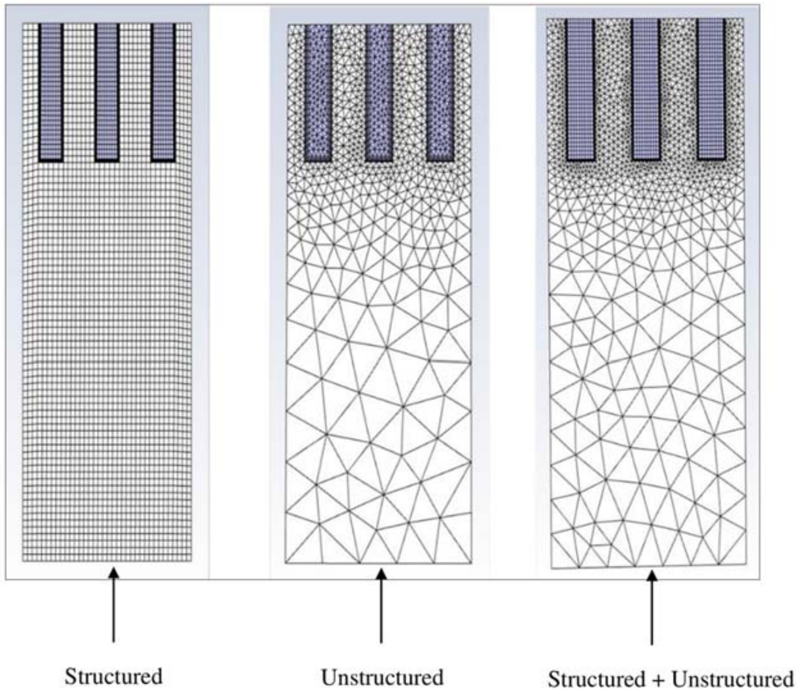

Fig. 3 Grids generated for the study

3.1 Comparison of Nano-Liquid Metal Fluid With Water-Based Nanofluid. The current study comprises a comparison study of liquid metal-based nanofluids with water-based nanofluids. The first comparison is conducted using different liquid metals having Al_2O_3 as particles with water–Al_2O_3 nanofluids. The average heat transfer coefficient of water–Al_2O_3 is taken from experimental studies reported in Ref. [37]. The presented analysis is conducted having similar boundary conditions for a range of Reynolds number (Re = 150–750). The volume fraction of nanoparticles is kept consistent ($\alpha_p = 0.02$). The fluid inlet temperature is taken as $T_{in} = 20$ °C, and a constant heat flux of ($q_f = 100$ W/cm^2) is applied at the bottom of the heat sink. Following the similar boundary conditions, pressure drop due to fluid delivery inside the microchannels are compared.

The results presented in Fig. 5 shows that the average heat transfer coefficient of liquid metal-based nanofluids is much superior compared to that of water-based nanofluid. At lower Reynolds number, all of the coolants show quite similar thermal performance. But while increasing the flow Reynolds number, an increase in the average heat transfer coefficient was noticed for all the liquid metal-based nanofluids. GaIn displays the highest heat transfer coefficient due to its better thermal conductivity. Figure 6 displays the comparison of pressure drop for different base fluids with water-based nanofluids. It is noticed that liquid metal-based nanofluids result in more pressure drop with respect to the water-based nanofluid due to the high density and viscosity of liquid metals compared to that of water.

Although water-based nanofluid shows higher pressure drop than Ga- and EGaIn-based nanofluids, conclusions cannot be reached from this comparison since with the same Reynolds number, the inlet velocity of water-based nanofluid is far more than liquid metal-based nanofluids due to much lower density and viscosity of water. Thus, further analysis is made with the same inlet velocity to obtain the overall picture of the thermal and hydraulic performance. The results presented in Fig. 7 show quite identical thermal performance as shown in Fig. 5. The average heat transfer coefficient of water-based nanofluid does not show much improvements at higher velocity. On the other hand, liquid metal-based nanofluids show much improvement in thermal performance at higher velocity. In the

Table 5 Solution comparison with different grids

Grid type	Number of elements	Outlet temperature (numerical)	Outlet temperature (experimental)	Error
Structured	1.4 million	40.8941 °C	39.339 °C	3.953%
	3.7 million	40.8935 °C	39.339 °C	3.952%
	5.7 million	40.8931 °C	39.339 °C	3.951%
Unstructured	2.4 million	40.8945 °C	39.339 °C	3.954%
	4.7 million	40.8941 °C	39.339 °C	3.953%
	6.7 million	40.8921 °C	39.339 °C	3.948%
Unstructured + structured	3.7 million	40.8934 °C	39.339 °C	3.951%
	5.4 million	40.8932 °C	39.339 °C	3.951%
	6.5 million	40.8929 °C	39.339 °C	3.950%

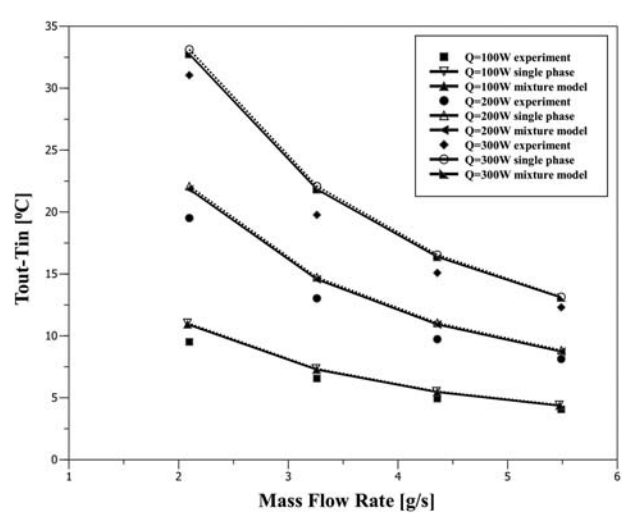

Fig. 4 Comparison of numerical data with experimental data

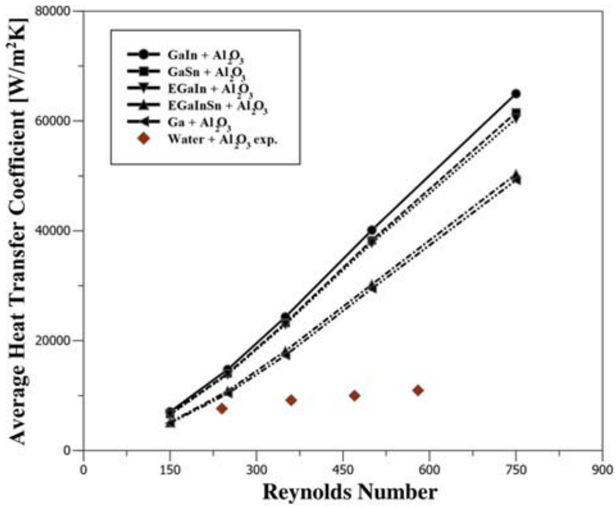

Fig. 5 Comparison of thermal performance between liquid metal-based nanofluids with water-based nanofluid

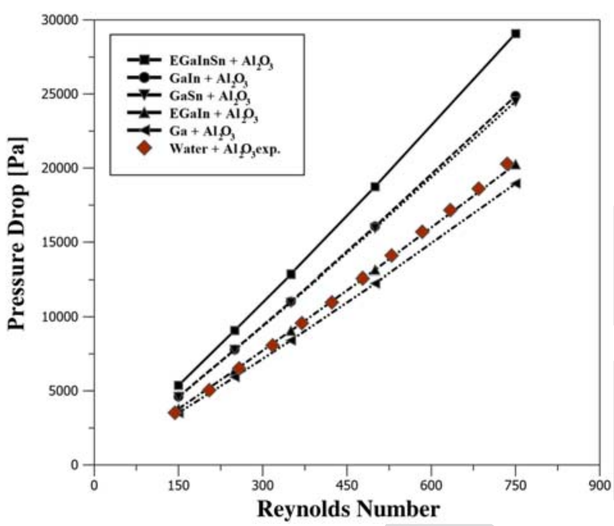

Fig. 6 Comparison of hydraulic performance between liquid metal-based nanofluids with water-based nanofluid

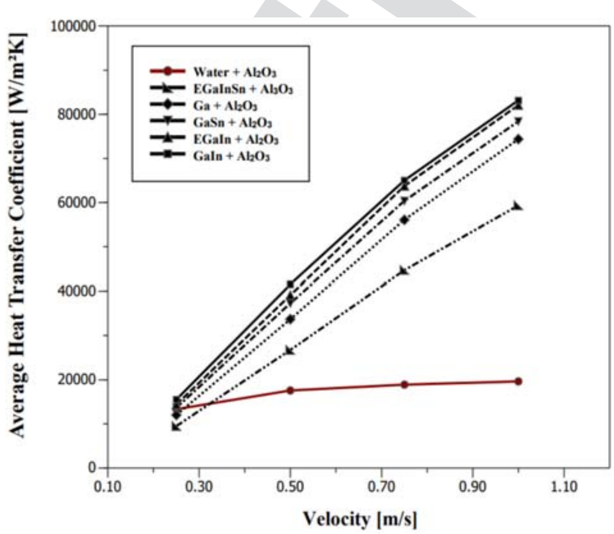

Fig. 7 Comparison of average heat transfer coefficient versus coolant inlet velocity

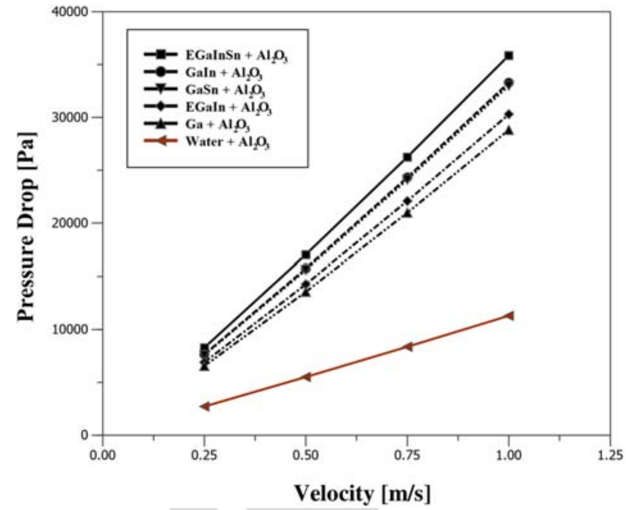

Fig. 8 Comparison of pressure drop versus coolant inlet velocity

case of pressure drop, as displayed in Fig. 8, liquid metal-based nanofluids require much more pumping power at the same inlet velocities than water-based nanofluid. This phenomenon occurs due to much higher density and viscosity of the liquid metals than water. Among them, EGaInSn-based nanofluids require the most pumping power, and Ga-based nanofluids require the lowest pumping power.

Then, to compare the thermal performance of nano-liquid metal fluid with water-based nanofluids, the substrate wall temperature and the bulk mean fluid temperature is evaluated. The analysis has been carried out for Re = 500 and volume fraction ($\alpha_p = 0.02$).

As displayed in Figs. 9 and 10, GaIn-based nanofluids tend to reduce the surface temperature and the fluid mean temperature decreases among the liquid metal-based nanofluids, but as water has a substantial higher velocity for the same Reynolds number than liquid metals because of considerably lower density, water-based nanofluids tends to reduce these temperatures much lower. As presented in Table 3, the specific heat of water is quite large than other coolants used in this study, which plays an effective role in maintaining a lower temperature in the substrate material. So, it has been found that although water-based nanofluid has lower heat transfer coefficient at the same Reynolds number, they

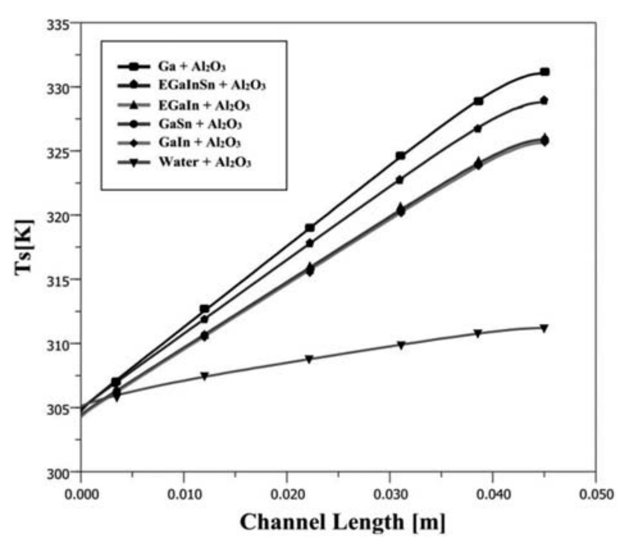

Fig. 9 Substrate wall temperature along the channel length

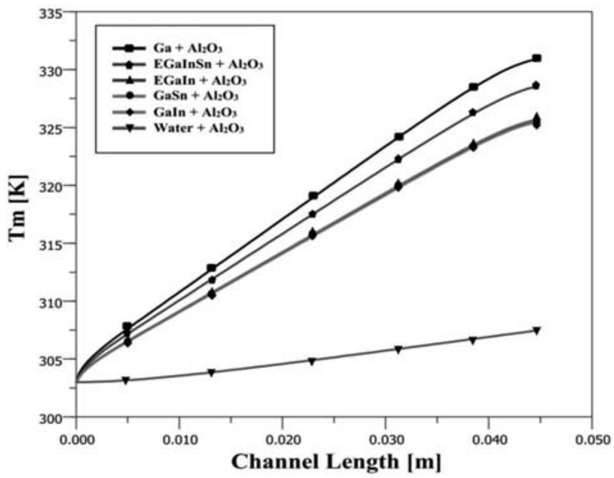

Fig. 10 Fluid mean temperature along the channel length

possess the ability to keep the surface temperature at a lower value than liquid metal-based nanofluids. On the other hand, liquid metal-based nanofluids though possessing a higher heat transfer coefficient shows low performance while keeping the substrate temperature below a certain point. All the results show consistency with the increasing temperature along with the length of the channel, as suggested in Ref. [36].

3.2 Comparison of the Influence of Different Nanoparticles. After comparing different base fluids, the effect of different nanoparticles on the MCHS performance has been carried out. Four different types of nanoparticles of the same concentration of 2% are used with the liquid metal solvents, and the average heat transfer coefficient is calculated for all the combinations. The comparison is presented in Fig. 11. At a lower Reynolds number, all the particles display the same thermal characteristics. But at higher Reynolds number, a difference in the thermal performance can be seen. It can be noticed that irrespective of the base fluid, CNT particle-based nanofluids provide a higher thermal performance because of their higher thermal conductivity. From the comparison study, it can be found that the GaIn–CNT mixture exhibits the highest thermal performance. For GaIn as the base fluid and Re = 750, CNT particle has an enhancement of 12.48%, 9.48%, and 8.79% over Al_2O_3, Cu, and diamond particles.

In case of hydraulic performance, incorporation of different particles of the same diameter at the same concentration of 2% results in an unnoticeable change in viscosity and density. As a consequence, the change in pressure drop and pumping power is also trivial and insignificant. The effect of different particles on pressure drop, pumping power, and friction factor for GaIn-based nanofluids are presented in Table 6.

3.3 Comparison of Nanoparticles Volume Fraction Influence on Heat Sink Performance. Further study of particle concentration ranging from 1% to 5% has been carried out for GaIn–CNT due to its outstanding thermal performance. The range has been selected based on the fact that for higher particle concentration, the hydraulic and thermal performance effect is very negligible in microchannel heat sink. Also, it is quite hard to predict the nature of the flow at very large volume fractions due to agglomeration of particles and clogging of the small channels in higher concentration.

Figure 12 presents the effect of nanoparticle volume fraction on the convective heat transfer coefficient for GaIn–CNT at Reynolds number ranging from Re = 250–750 and $q_f = 100$ W/m^2. It has been found from the results that with the increasing concentration, the thermal conductivity of the mixture also increases and hence the heat transfer coefficient increases although the increment is not linear. For Re = 500, the increasing concentration from 1% to 2% results in an increase in the heat transfer coefficient by 5.35%, whereas for the same magnitude of increment from 4% to 5%, the heat transfer coefficient increases by 2.73%. So, the thermal performance enhancement gradually decreases with the increasing concentration and becomes negligible for a higher concentration. For the increasing Reynolds number, the concentration difference has a higher effect on thermal performance. This finding suggests similarity with the literature [36] about the effect of the Reynolds number on thermal performance for different particle concentrations.

Figure 13 presents the effect of particle concentration on pressure drop and corresponding pumping power. With the increasing particle concentration, the viscosity of the mixture also increases, which results in higher pressure drop and pumping power for the same Reynolds number. But the effect of concentration increment on hydraulic performance decreases at higher particle concentration similar as seen regarding thermal performance. For Re = 500, increasing concentration from 1% to 2% results in 3.8% viscosity increase and corresponding 3.09% increase in pressure drop, where the same increment of concentration from 4% to 5% results in 2.27% increase in viscosity and corresponding 2.25% increase in pressure drop.

The effect of the particle concentration on the substrate wall temperature and bulk mean fluid temperature is presented in Figs. 14 and 15. The increase in the particle concentration in a nanofluid increases its thermal conductivity. Thus, with the increasing particle concentration in a nanofluid, its heat transfer capacity increases. Consecutively, the substrate wall temperature and bulk fluid temperature decrease. The reduced amplitude is enlarged with the volume fraction increment although the variation is trivial due to the small size of microchannels. These findings suggest that although with the increasing particle concentration, the heat transfer coefficient increases rapidly but due to the compactness of the heat sink, surface and bulk fluid temperature variations are negligible; hence, the cooling effectiveness is indistinguishable.

3.4 Performance Evaluation Criterion. While comparing the thermal performance of any coolants in microchannel heat sinks, the most common issue to deal with is the mismatch in the thermophysical properties of the coolants. The difference in certain properties like density and thermal conductivity can deviate the actual findings of the comparison study. Since, for a similar flow Reynolds number, the inlet velocity of water-based nanofluids is far greater than liquid metal-based nanofluids, the apparent results might be misleading. Conversely, an apparent thermal performance increment can easily be nullified considering the cost of extra pumping power requirements for any coolants. Thus, from the energetic considerations, performance evaluation criterion (PEC) is utilized in this study to model the overall performance of different coolants. PEC is expressed as follows [44–46]:

$$\mathrm{PEC} = \frac{\dot{m} c_p (T_{out} - T_{in})}{V \Delta P} \tag{28}$$

where $\dot{m}$ is the mass flowrate, c_p is the specific heat, T_{out} and T_{in} are the outlet and inlet temperature of the coolants, respectively, V represents the volumetric flowrate, and ΔP represents the pressure drop.

To compare the overall performance of liquid metal-based nanofluids, performance evaluation criterion for different liquid metal-based nanofluids are compared with 2% Al_2O_3–water coolants. The volume fraction of nanoparticles is kept consistent (α_p = 0.02). The fluid inlet temperature is taken as (T_{in} = 20 °C) and a constant heat flux of (q_f = 100 W/cm^2) is applied at the bottom of the heat sink. From Fig. 16, it has been found that for the same concentration of 2%, the increase of the Reynolds number results in the reduction of PEC. This changing tendency shows that the energetic

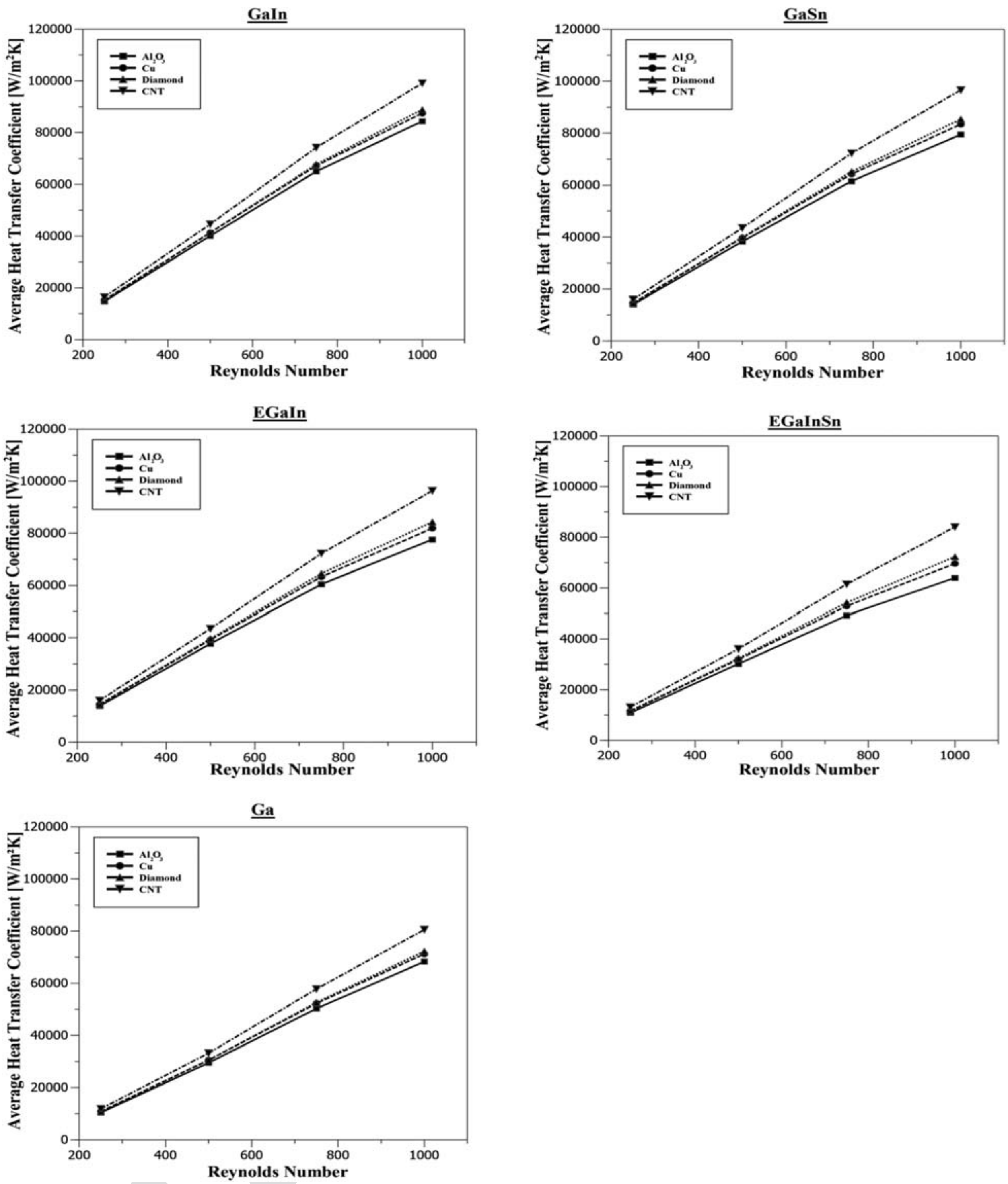

Fig. 11 Comparison of thermal performance between different nanoparticles

cost of pumping power is much higher than the corresponding heat transfer enhancement benefit [36]. At a lower Reynolds number, the thermal performance of Nano is dominating. For this reason, the variation in different base fluid's "PEC" is noticeable. But with the increasing Reynolds number, the thermal effect lessens in respect of pumping performance and the variation in PEC reduces. Liquid metal-based nanofluids have considerably higher PEC than water-based nanofluid irrespective of the Reynolds number. This indicates that Ga has the higher thermal benefit, considering the cost of pumping power.

Next, PEC has been applied to assess the overall performance of a particle's concentration variation. GaIn–CNT nano-liquid metal fluid has been used here as coolants. The fluid inlet temperature is taken as ($T_{in} = 20\,°C$), and a constant heat flux of ($q_f = 100\ W/cm^2$) is applied at the bottom of the heat sink. Figure 17 shows the variation of PEC with Reynolds number and nanoparticles volume fraction. It has been found that, with the increase of Reynolds number, the PEC decreases. This changing tendency shows that the energetic cost of pumping power is becoming much higher than the corresponding heat transfer enhancement

Table 6 Hydraulic performance with different nanoparticles suspended in GaIn liquid metal

		Particle			
Reynolds number		Al_2O_3	Cu	CNT	Cu
Re = 500	Pressure drop (kPa)	16.067	16.084	16.059	16.065
	Friction factor	0.03737911	0.036792227	0.037599858	0.037386522
	Pumping power (10^{-3} W)	30.329694	30.36254	30.315348	30.327051
Re = 750	Pressure drop (kPa)	24.867	24.903	24.851	24.864
	Friction factor	0.025712882	0.025318185	0.02586022	0.025716912
	Pumping power (10^{-3} W)	70.414745	70.516114	70.369157	70.405684
Re = 1000	Pressure drop (kPa)	33.952	34.041	33.920	33.961
	Friction factor	0.019747277	0.019467097	0.019854626	0.019757975
	Pumping power (10^{-3} W)	128.184723	128.520734	128.064288	128.217569

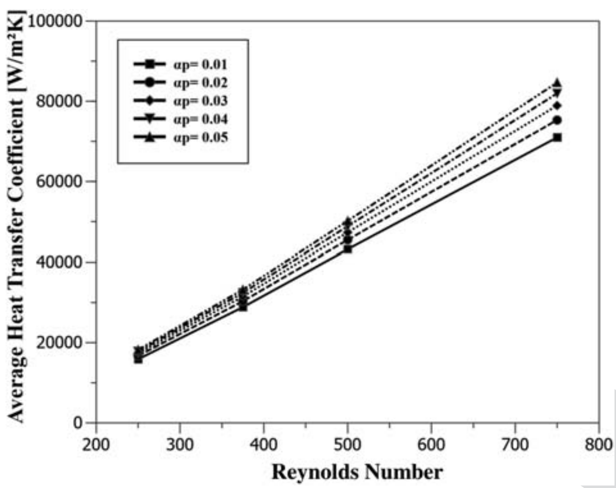

Fig. 12 Comparison of thermal performance with different volume fractions of nanofluids

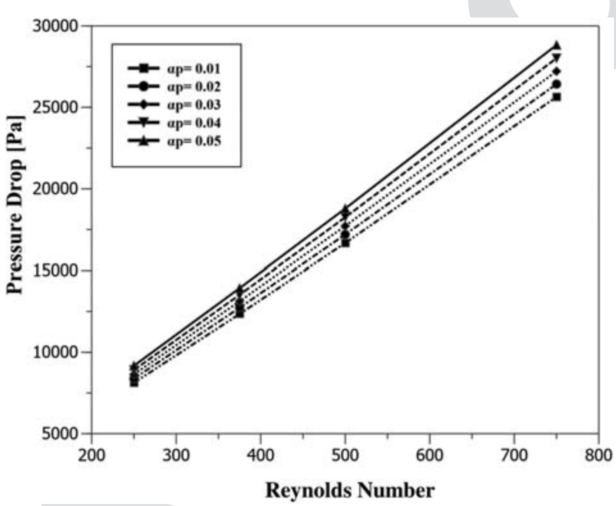

Fig. 13 Comparison of hydraulic performance with different volume fractions of nanofluids

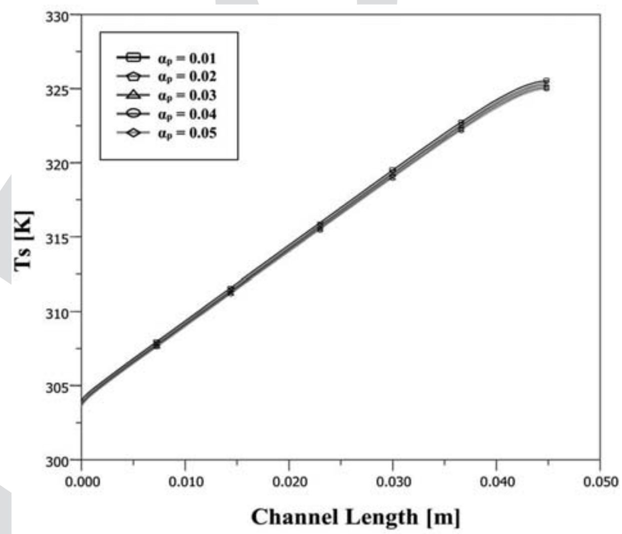

Fig. 14 Comparison of substrate wall temperature with different particle concentrations

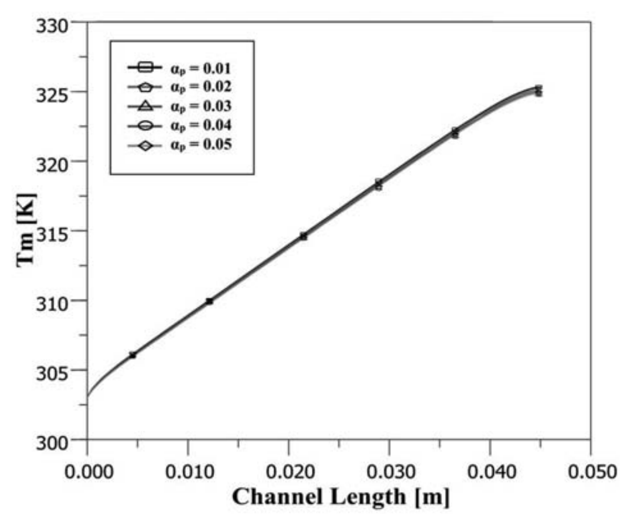

Fig. 15 Comparison of bulk fluid mean temperature with different particle concentrations

benefit. The findings presented in Ref. [36] also agree with this phenomenon regarding the reduction of PEC with the increase in Reynolds number. The reduced amplitude of PEC varies for different concentrations. It has been found for lower volume fractions of nanofluids; the PEC curve is much steeper, which indicates that overall thermal performance reduction considering pumping cost increment is larger for lower concentration with the increasing Reynolds number. It is also evident from the figure that for higher Reynolds number, the influence of concentration on the thermal, hydraulic, and overall performance is indistinguishable.

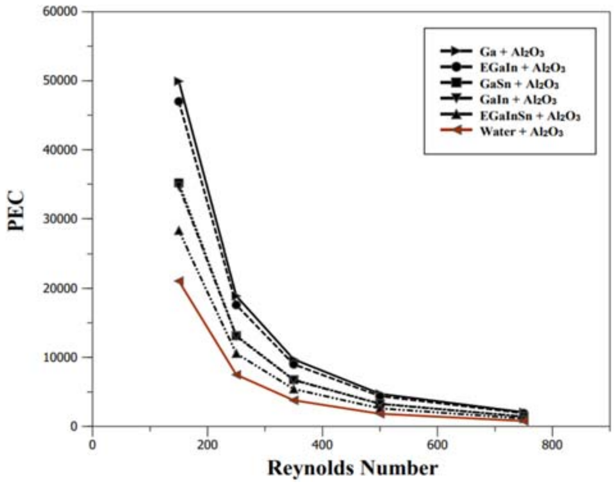

Fig. 16 Comparison of PEC between nano-liquid metal fluids and water-based nanofluid

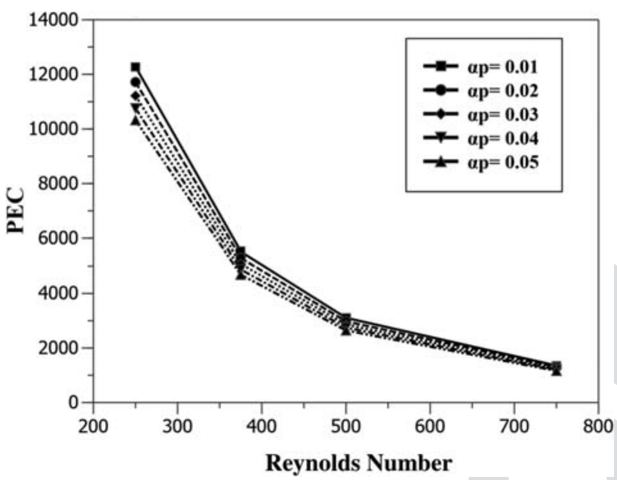

Fig. 17 Comparison of PEC with different volume fractions of nanofluids

3.5 Limitations of Numerical Investigation. As our whole study is based on numerical simulations, despite having good consistency and accuracy with reference experimental data [37], we have several limitations and constraints. It has been suggested that as liquid metal has large surface tension, a much larger volume fraction of nanoparticles can be added to the liquid metal [36]. Still the preparation and implementation of nano-liquid metal fluid in such small-scale applications has not been carried out experimentally. Thus, the feasibility and tangibility of the proposed cooling technology in MCHS is uncertain. The limitations of our numerical model are as follows:

- There is no universal model for the determination of nanofluid mixture properties. Implementation of each model depends on the combination and context of the problem.
- Since the channels of the microchannel heat sink are very narrow, it is very challenging to calculate the fin efficiency accurately.
- Prediction of the flow field and heat transfer phenomena for high velocity flow and high source heat flux is very challenging and intangible.
- High surface area to volume ratio of nanoparticles provides a very high surface energy. To minimize its surface energy, the nanoparticles create agglomeration. The physical phenomena of agglomeration have a disrupted effect on the overall performance of the sink by creating a huge disturbance in the flow field of MCHS. Sonicating or adding surfactant might help for a short period of time, but it will not be effective for the long term.

4 Conclusion and Recommendation

This study presented the incorporation of nano-liquid metal fluid as the cooling medium in MCHS. This serves as a state-of-the-art technology regarding the cooling solution for miniaturized electronic components. This numerical investigation has contributed to this field with a detailed performance comparison of different conventionally used liquid metal and nanoparticle combinations along with the particle concentration study. The inferences from investigations are as follows:

- Nano-liquid meal fluids display better thermal performance compared to the base fluid, especially at high Reynolds number, and among them, GaIn-based nano-liquid metal fluid displays the most heat transfer coefficient. For the same nanoparticle Al_2O_3 and $Re = 600$ and volume fraction ($\alpha_p = 0.02$), GaIn-based nanofluids display 3.41 times higher heat transfer coefficient than conventional water–Al_2O_3 nanofluid. Also, the increasing Reynolds number from 300 to 600 results in an increment of 131.58% heat transfer coefficient for GaIn-based Nanofluids, where the same increment in Reynolds number results in only 31.23% increase of the heat transfer coefficient for water-based nanofluids.
- Considering the hydraulic performance, Ga- and EGaIn-based nanofluids requires the least pumping power for the same Reynolds number among other liquid metal-based nanofluids. However, comparing the overall performance (PEC), Ga-based nanofluids are more suitable considering energy efficiency. But regarding thermal performance, GaIn-based nanofluids exhibit the highest performance.
- CNT particle-based nanofluids display better thermal performance than conventional nanoparticles due to their high thermal conductivity. For GaIn as base fluid and $Re = 750$, CNT particles have an enhancement of 12.48%, 9.48%, and 8.79% over Al_2O_3, Cu, and diamond particles. It has been determined that the GaIn–CNT mixture exhibits the highest thermal performance. For the same Reynolds number, the GaIn–CNT mixture has a heat transfer coefficient increment of 2.68%, 17.19%, 22.16%, and 2.62% over CNT particle-based EGaIn, EGaInSn, Ga, and GaSn liquid metal, respectively.
- With the increasing particle concentration, heat transfer coefficient and pressure drop across the channel both increase due to the increase in the mixture's thermal conductivity and viscosity, respectively. Although the increment is nonlinear and the rate of increment decreases with the increasing particle concentration. Considering overall performance, the increasing concentration results in a reduction of PEC, which indicates the energetic cost of pumping power being much higher than the corresponding heat transfer enhancement. For higher Reynolds number, the influence of concentration on the thermal, hydraulic, and overall performance is indistinguishable.
- Despite their ability to enhance the single-phase heat transfer coefficient due to the increased thermal conductivity, the overall cooling effectiveness of particle concentration increment is relatively minuscule.

In this present study, optimal nano-liquid metal fluid combinations have been determined considering different perspectives. Optimal range of Reynolds number and particle concentration has been analyzed for significant thermal performance improvements. This has built the foundation for future experimental work regarding the use of nano-liquid metal fluid in electronic component cooling. Although this technology is constrained by the expense of the preparation of nano-liquid metal fluids, it is an inception to reach ultimate cooling solutions and work toward the solution of bottleneck cooling issues associated with miniaturization of electronic components.

Conflict of Interest

There are no conflicts of interest.

Nomenclature

f = friction factor
h = heat transfer coefficient (W/m^{2}K)
k = thermal conductivity (W/m K)
H = height of the heat sink (m)
L = length of the heat sink (m)
N = number of channels
Q = total heat flux applied at the bottom of the heat sink (W)
V = volumetric flowrate (m^3/s)
W = width of the heat sink (m)
W = pumping power (W)
$\dot{m}$ = mass flowrate (kg/s)
c_p = specific heat capacity (J/kg K)
q_f = heat flux per unit area (W/m^2)
t_b = thickness of the base of the heat sink (m)
A_{fin} = surface area of a channel wall (m^2)
A_{fin} = area of the fin (m^2)
A_{in} = area of the inlet (m^2)
H_c = height of a channel (m)
D_h = hydrodynamic diameter
W_c = width of a single channel (m)
W_{fin} = width of the channel wall (m)
L_{fin} = length of the fin (m)
P_{in} = pressure of fluid at the inlet (Pa)
T_{in} = temperature at the inlet (K)
T_m = bulk mean fluid temperature (K)
U_{in} = inlet velocity (m/s)
V_m = mass averaged velocity
ΔP = pressure drop (Pa)
ΔT_{btd} = base fluid temperature difference (K)
η_{fin} = fin efficiency
Re = Reynolds number
Nu = Nusselt number

Greek Symbols

s = viscosity (Pa s)
ρ = density (kg/m^3)
φ = volume fraction of nanoparticles

Subscripts

bf = base fluid
c = channel
f = fluid
fin = channel wall
in = inlet
k = phase
m = mixture
nf = nanofluid
p = nanoparticle
s = solid

References

[1] Tuckerman, D. B., and Pease, R. F. W., 1981, "High-Performance Heat Sinking For VLSI," IEEE Electron Device Lett., **2**(5), pp. 126–129.
[2] Shah, R. K., 2006, "Advances in Science and Technology of Compact Heat Exchangers," Heat Transfer Eng., **27**(5), pp. 3–22.
[3] Popescu, T., Marinescu, M., Pop, H., Popescu, G., and Feidt, M., 2012, "Microchannel Heat Exchangers—Present and Perspectives," UPB Sci. Bull. Ser. D: Mech. Eng., **74**(3), pp. 55–70.
[4] Naqiuddin, N. H., Saw, L. H., Yew, M. C., Yusof, F., Ng, T. C., and Yew, M. K., 2018, "Overview of Micro-Channel Design for High Heat Flux Application," Renewable Sustainable Energy Rev., **82**, pp. 901–914.
[5] Hadad, Y., Ramakrishnan, B., Pejman, R., Rangarajan, S., Chiarot, P. R., Pattamatta, A., and Sammakia, B., 2019, "Three-Objective Shape Optimization and Parametric Study of a Micro-Channel Heat Sink With Discrete Non-Uniform Heat Flux Boundary Conditions," Appl. Therm. Eng., **150**, pp. 720–737.
[6] Chandra, S., and Prakash, O., 2016, "Heat Transfer in Microchannel Heat Sink: Review," International Conference on Recent Advances in Mechanical Engineering, Oct.
[7] Li, X., and Jia, L., 2015, "The Investigation On Flow Boiling Heat Transfer Of R134a in Micro-Channels," J. Therm. Sci., **24**(5), pp. 452–462.
[8] Ali, R., Palm, B., and Maqbool, M. H., 2012, "Flow Boiling Heat Transfer of Refrigerants R134A and R245fa in a Horizontal Micro-Channel," Exp. Heat Transfer, **25**(3), pp. 181–196.
[9] Dong, T., Yang, Z., Bi, Q., and Zhang, Y., 2008, "Freon R141b Flow Boiling in Silicon Microchannel Heat Sinks: Experimental Investigation," Heat Mass Transfer, **44**(3), pp. 315–324.
[10] Choi, S. U. S., 2009, "Nanofluids: From Vision to Reality Through Research," ASME J. Heat Transfer, **131**(3), pp. 1–9.
[11] Kim, S. J., Bang, I. C., Buongiorno, J., and Hu, L. W., 2007, "Surface Wettability Change During Pool Boiling of Nanofluids and Its Effect on Critical Heat Flux," Int. J. Heat Mass Transfer, **50**(19–20), pp. 4105–4116.
[12] Masuda, H., Ebata, A., Teramae, K., and Hishinuma, N., 1993, "Alteration of Thermal Conductivity and Viscosity of Liquid by Dispersing Ultra-Fine Particles. Dispersion of Al2O3, Sio2 and Tio2 Ultra-Fine Particles," Netsu Bussei, **7**(4), pp. 227–233.
[13] Huminic, G., and Huminic, A., 2012, "Application of Nanofluids in Heat Exchangers: A Review," Renewable Sustainable Energy Rev., **16**(8), pp. 5625–5638.
[14] Ho, C. J., Wei, L. C., and Li, Z. W., 2010, "An Experimental Investigation of Forced Convective Cooling Performance of a Microchannel Heat Sink With Al2O3/Water Nanofluid," Appl. Therm. Eng., **30**(2–3), pp. 96–103.
[15] Kumar, P. C. M., and Kumar, C. M. A., 2020, "Numerical Study on Heat Transfer Performance Using Al2O3/Water Nanofluids in Six Circular Channel Heat Sink For Electronic Chip," Mater. Today: Proc., **21**, pp. 194–201.
[16] Moraveji, M. K., and Ardehali, R. M., 2013, "CFD Modeling (Comparing Single and Two-Phase Approaches) on Thermal Performance of Al2O3/Water Nanofluid in Mini-Channel Heat Sink," Int. Commun. Heat Mass Transfer, **44**, pp. 157–164.
[17] Alfaryjat, A., Gheorghian, A. T., Nabbat, A., Ştefănescu, M. F., and Dobrovicescu, A., 2018, "The Impact of Different Base Nanofluids on the Fluid Flow and Heat Transfer Characteristics in Rhombus Microchannels Heat Sink," UPB Sci. Bull. Ser. D: Mech. Eng., **80**(1), pp. 181–194.
[18] Razali, A. A., Sadikin, A., and Ibrahim, S. A., 2017, "Heat Transfer of Al2O3 Nanofluids in Microchannel Heat Sink," AIP Conf. Proc., **1831**, p. 020050.
[19] Sivakumar, A., Alagumurthi, N., and Senthilvelan, T., 2017, "Effect of Serpentine Grooves on Heat Transfer Characteristics of Microchannel Heat Sink With Different Nanofluids," Heat Transf.—Asian Res., **46**(3), pp. 201–217.
[20] Azizi, Z., Alamdari, A., and Malayeri, M. R., 2015, "Convective Heat Transfer of Cu-Water Nanofluid in a Cylindrical Microchannel Heat Sink," Energy Convers. Manag., **101**, pp. 515–524.
[21] Jang, S. P., and Choi, S. U. S., 2006, "Cooling Performance of a Microchannel Heat Sink With Nanofluids," Appl. Therm. Eng., **26**(17–18), pp. 2457–2463.
[22] Halelfadl, S., Adham, A. M., Mohd-Ghazali, N., Maré, T., Estellé, P., and Ahmad, R., 2014, "Optimization of Thermal Performances and Pressure Drop of Rectangular Microchannel Heat Sink Using Aqueous Carbon Nanotubes Based Nanofluid," Appl. Therm. Eng., **62**(2), pp. 492–499.
[23] Martínez, V. A., Vasco, D. A., García-Herrera, C. M., and Ortega-Aguilera, R., 2019, "Numerical Study of Tio2-Based Nanofluids Flow in Microchannel Heat Sinks: Effect of the Reynolds Number and the Microchannel Height," Appl. Therm. Eng., **161**, p. 114130.
[24] Song, H., Kim, T., Kang, S., Jin, H., Lee, K., and Yoon, H. J., 2020, "Ga-Based Liquid Metal Micro/Nanoparticles: Recent Advances and Applications," Small, **16**(12), pp. 1–21.
[25] Smither, R. K., Forster, G. A., Kot, C. A., and Kuzay, T. M., 1988, "Liquid Gallium Metal Cooling For Optical Elements With High Heat Loads," Nucl. Inst. Methods Phys. Res. A, **266**(1–3), pp. 517–524.
[26] Sawada, T., Netchaev, A., Ninokata, H., and Endo, H., 2000, "Gallium-Cooled Liquid Metallic-Fueled Fast Reactor," Prog. Nucl. Energy, **37**(1–4), pp. 313–319.
[27] Liu, Y., Chen, H. F., Zhang, H. W., and Li, Y. X., 2015, "Heat Transfer Performance of Lotus-Type Porous Copper Heat Sink With Liquid Gainsn Coolant," Int. J. Heat Mass Transfer, **80**, pp. 605–613.
[28] Muhammad, A., Selvakumar, D., Iranzo, A., Sultan, Q., and Wu, J., 2020, "Comparison of Pressure Drop and Heat Transfer Performance for Liquid Metal Cooled Mini-Channel With Different Coolants and Heat Sink Materials," J. Therm. Anal. Calorim., **141**(1), pp. 289–300.
[29] Muhammad, A., Selvakumar, D., and Wu, J., 2020, "Numerical Investigation of Laminar Flow and Heat Transfer in a Liquid Metal Cooled Mini-Channel Heat Sink," Int. J. Heat Mass Transfer, **150**, p. 119265.
[30] Liu, H. L., An, X. K., and Wang, C. S., 2017, "Heat Transfer Performance of T-Y Type Micro-Channel Heat Sink With Liquid Gainsn Coolant," Int. J. Therm. Sci., **120**, pp. 203–219.
[31] Sarowar, M. T., 2021, "Numerical Analysis of a Liquid Metal Cooled Mini Channel Heat Sink With Five Different Ceramic Substrates," Ceram. Int., **47**(1), pp. 214–225.
[32] Barbier, F., and Blanc, J., 1999, "Corrosion of Martensitic and Austenitic Steels in Liquid Gallium," J. Mater. Res., **14**(3), pp. 737–744.

[33] Deng, Y. G., and Liu, J., 2009, "Corrosion Development Between Liquid Gallium and Four Typical Metal Substrates Used in Chip Cooling Device," Appl. Phys. A, **95**(3), pp. 907–915.

[34] Tawk, M., Avenas, Y., Kedous-Lebouc, A., and Petit, M., 2013, "Numerical and Experimental Investigations of the Thermal Management of Power Electronics With Liquid Metal Mini-Channel Coolers," IEEE Trans. Ind. Appl., **49**(3), pp. 1421–1429.

[35] Ma, K. Q., and Liu, J., 2007, "Nano Liquid-Metal Fluid as Ultimate Coolant," Phys. Lett. A, **361**(3), pp. 252–256.

[36] Zhou, X., Li, X., Cheng, K., and Huai, X., 2018, "Numerical Study of Heat Transfer Enhancement of Nano Liquid-Metal Fluid Forced Convection i Circular Tube," ASME J. Heat Transfer, **140**(8), p. 081901.

[37] Lee, J., and Mudawar, I., 2007, "Assessment of the Effectiveness of Nanofluids for Single-Phase and Two-Phase Heat Transfer in Micro-Channels," Int. J. Heat Mass Transfer, **50**(3–4), pp. 452–463.

[38] Moraveji, M. K., Darabi, M., Haddad, S. M. H., and Davarnejad, R., 2011, "Modeling of Convective Heat Transfer of a Nanofluid in the Developing Region of Tube Flow With Computational Fluid Dynamics," Int. Commun. Heat Mass Transfer, **38**(9), pp. 1291–1295.

[39] Mansour, R. B., Galanis, N., and Nguyen, C. T., 2007, "Effect of Uncertainties in Physical Properties on Forced Convection Heat Transfer With Nanofluids," Appl. Therm. Eng., **27**(1), pp. 240–249.

[40] Khanafer, K., Vafai, K., and Lightstone, M., 2003, "Buoyancy-Driven Heat Transfer Enhancement in a Two-Dimensional Enclosure Utilizing Nanofluids," Int. J. Heat Mass Transfer, **46**(19), pp. 3639–3653.

[41] Moraveji, M. K., and Hejazian, M., 2012, "Modeling of Turbulent Forced Convective Heat Transfer and Friction Factor in a Tube for Fe 3o 4 Magnetic Nanofluid With Computational Fluid Dynamics," Int. Commun. Heat Mass Transfer, **39**(8), pp. 1293–1296.

[42] El-Batsh, H. M., Doheim, M. A., and Hassan, A. F., 2012, "On the Application of Mixture Model for Two-Phase Flow Induced Corrosion in a Complex Pipeline Configuration," Appl. Math. Model., **36**(11), pp. 5686–5699.

[43] Moghari, R. M., Akbarinia, A., Shariat, M., Talebi, F., and Laur, R., 2011, "Two Phase Mixed Convection Al2O3-Water Nanofluid Flow in an Annulus," Int. J. Multiphase Flow, **37**(6), pp. 585–595.

[44] Bianco, V., Manca, O., and Nardini, S., 2014, "Performance Analysis of Turbulent Convection Heat Transfer of Al2O3 Water-Nanofluid in Circular Tubes at Constant Wall Temperature," Energy, **77**, pp. 403–413.

[45] Ferrouillat, S., Bontemps, A., Ribeiro, J. P., Gruss, J. A., and Soriano, O., 2011, "Hydraulic and Heat Transfer Study of SiO2/Water Nanofluids in Horizontal Tubes With Imposed Wall Temperature Boundary Conditions," Int. J. Heat Fluid Flow, **32**(2), pp. 424–439.

[46] Roy, G., Gherasim, I., Nadeau, F., Poitras, G., and Nguyen, C. T., 2012, "Heat Transfer Performance and Hydrodynamic Behavior of Turbulent Nanofluid Radial Flows," Int. J. Therm. Sci., **58**, pp. 120–129.